AGU100 ADVANCING EARTH AND SPACE SCIENCE

Geophysical Research Letters

RESEARCH LETTER

10.1029/2018GL077937

The MJO-SSW Teleconnection: Interaction Between MJO-Forced Waves and the Midlatitude Jet

Wanying Kang[1] **and Eli Tziperman**[1,2]

[1]School of Engineering and Applied Sciences, Harvard University, Cambridge, MA, USA, [2]Department of Earth and Planetary Sciences, Harvard University, Cambridge, MA, USA

Key Points:

- SSW frequency is affected by MJO amplitude and longitudinal range which are both predicted to change
- MJO-SSW teleconnection is dominated by response of midlatitude jet and stationary waves to the MJO
- MJO-forced wave eddy momentum transport drives the response of midlatitude jet and stationary waves

Supporting Information:

- Supporting Information S1

Correspondence to:
W. Kang,
wanyingkang@g.harvard.edu

Citation:
Kang, W., & Tziperman, E. (2018). The MJO-SSW teleconnection: Interaction between MJO-forced waves and the midlatitude jet. *Geophysical Research Letters*, *45*, 4400–4409. https://doi.org/10.1029/2018GL077937

Received 17 DEC 2017
Accepted 9 APR 2018
Accepted article online 19 APR 2018
Published online 5 MAY 2018

Abstract The Madden-Julian Oscillation (MJO) was shown to affect both present-day sudden stratospheric warming (SSW) events in the Arctic and their future frequency under global warming scenarios, with implications to the Arctic Oscillation and midlatitude extreme weather. This work uses a dry dynamic core model to understand the dependence of SSW frequency on the amplitude and longitudinal range of the MJO, motivated by the prediction that the MJO will strengthen and broaden its longitudinal range in a warmer climate. We focus on the response of the midlatitude jets and the corresponding generated stationary waves, which are shown to dominate the response of SSW events to MJO forcing. Momentum budget analysis of a large ensemble of spinup simulations suggests that the climatological jet response is driven by the MJO-forced meridional eddy momentum transport. The results suggest that the trends in both MJO amplitude and longitudinal range are important for the prediction of the midlatitude jet response and for the prediction of SSWs in a future climate.

Plain Language Summary Sudden stratospheric warming (SSW) events occur in the Arctic stratosphere during winter approximately every other year, featuring an abrupt warming and a breakdown of the polar vortex. These events affect midlatitude extreme weather events and are therefore of a societal relevance, making it important to be able to predict a change in their frequency in a future climate change scenario. In the present climate, these events seem to be only weakly influenced by the Madden-Julian Oscillation (MJO), the dominant intraseasonal variability in the tropics. The authors have previously shown that a strengthening of the MJO, which is expected in a warmer future climate, may lead to more frequent SSW events. The mechanism behind such enhanced future SSW frequency is shown here to involve a nonlinear interaction of MJO-forced atmospheric waves with the midlatitude tropospheric jet. The waves make the midlatitude jet more asymmetric in longitude, therefore causing it to emit stronger stationary waves that reach the polar Arctic stratosphere, therefore leading to the more frequent occurrence of SSW events. This motivates studying this teleconnection between the tropical MJO and the Arctic SSW events using more detailed models, to increase our confidence in the prediction of future climate and weather regimes.

1. Introduction

Major sudden stratospheric warming (SSW) events occur in the Arctic stratosphere during winter at a frequency of about six events per decade. An SSW features a distorted or completely reversed stratospheric polar vortex, as well as tens of degrees warming within several days (Craig et al., 1959; Limpasuvan et al., 2004). In the month following an SSW event, the Northern Hemisphere is more likely to be in the negative phase of the Arctic Oscillation and also to experience more extreme weather (Kolstad et al., 2010; Mitchell et al., 2013; Thompson et al., 2002), motivating the need to understand what will affect the SSW frequency in a future climate.

The Madden-Julian Oscillation (MJO) was shown to be linked to SSW events at 3- to 4-week lag (Garfinkel et al., 2012; Kretschmer et al., 2017; Liu et al., 2014). Still, in the present climate, the MJO seems to have a relatively small effect on SSW and is dominated by many factors with a stronger effect on SSW events (e.g., Kretschmer et al., 2017). Kang and Tziperman (2017, 2018) showed that stronger MJO events, projected in global warming scenarios, can lead to a significant increase in the frequency of SSW events and analyzed the detailed teleconnection mechanism. Given that the MJO is projected to both get stronger (Arnold et al., 2013, 2014; Jones & Carvalho, 2006; Lee, 1999; Slingo et al., 1999) and to expand to a larger longitudinal range (Adames et al., 2017; Arnold et al., 2014; Chang et al., 2015) in a warmer climate, a robust prediction of a trend in the SSW frequency should take the MJO change into consideration.

Kang and Tziperman (2018, hereafter KT) showed that the effect of the MJO on the SSW frequency strongly depends on the zonal asymmetry of the midlatitude jet. In the Northern Hemisphere, the orography, land-sea contrast, and the zonal nonuniformity of the sea surface temperature force the midlatitude jet to tilt northward and to strengthen over the western ocean basins (Brayshaw et al., 2009, 2011; Tamarin & Kaspi, 2017). This background zonal asymmetry was found to contribute directly to an upward Eliassen-Palm flux (EP flux) (KT; see also Obrien et al., 1994) and to enhance the transmission of MJO-forced waves (KT). The jet exit regions, located in the East Pacific and Atlantic, were suggested to help the amplification, accumulation, and propagation of Rossby waves initiated from the tropics (Bao & Hartmann, 2014; Naoe et al., 1997; Simmons et al., 1983; Webster & Chang, 1988). In turn, a transient MJO forcing was also shown to trigger a stationary response in the midlatitudes, in both a shallow water model (Bao & Hartmann, 2014) and a dry dynamic core model (KT).

We explore here, using a dry dynamic core model with a realistic winter climatology, the response of the SSW frequency to MJO-like forcing with different amplitudes and different longitudinal ranges, motivated by prediction that the MJO will strengthen and broaden in longitude in a warmer climate (Adames et al., 2017; Arnold et al., 2013, 2014; Chang et al., 2015). We find that SSWs are significantly enhanced when the MJO forcing is restricted to the Indo-Pacific sector as observed, while the response is less significant for other longitudinal ranges. As for the mechanism, the response of the midlatitude jet and stationary waves to the MJO forcing is found to play a dominant role in determining the Arctic stratospheric response. To understand the jet response, we therefore examine the spin-up of the response when the MJO forcing is turned on, by running a large ensemble of short-term simulations, and identify the physical mechanisms behind the jet response. While this paper focuses on the response of SSW events to a strengthening of the MJO in order to isolate and understand this specific process, future changes to the other factors currently affecting SSW (e.g., Kretschmer et al., 2017) could be significant and perhaps even dominate those due to the MJO.

2. Methods

Model settings. A dry dynamical core model is used, with a similar configuration to that of Kang and Tziperman (2018). A realistic topography is used, and the background climatology is forced to the January climatology in a control Specified-Chemistry Whole Atmosphere Community Climate Model (Marsh et al., 2013) simulation, using the method of Hall (2000). We enhance the stratospheric vertical resolution to 18 levels (a total of 35 levels), to more realistically simulate SSWs, and run each simulation for 50 years to get robust statistics. In order to focus on the response of SSWs to future MJO changes, we use the same present-day atmospheric background for all experiments, although changes to the general circulation and overall thermodynamic structure of the atmosphere with climate change may affect the MJO effects on the Arctic stratosphere.

MJO-like forcing. The MJO-like forcing is set to a global $k = 1$ heating/cooling pattern, eastward propagating along the equator with 40-day period. The specified forcing amplitude ranges from 1 to 10 K/day, and the longitudinal range (window) of the forcing is set to one of four different configurations. Window A corresponds to circumglobal forcing, while windows B, C, and D are longitudinally restricted: window B corresponds to the Indo-Pacific sector (60–180° E) where the MJO is observed in the present climate, and window C (D) is shifted by 120° eastward (westward) from B. The response to window B forcing is meant to represent the observed MJO-SSW teleconnection, while the other windows are used to enhance our understanding of the role of the longitudinal position and extent of the MJO forcing. Each experiment is named [W][X], where [W] represents the window label and [X] represents the MJO-like forcing amplitude in kelvin per day. Additional details about the experiments' setup are given in supporting information Text S1.

Although we prescribe a $k = 1$ forcing pattern, the restriction to a specified longitudinal window of 120° longitude spreads the MJO power spectrum over $k = 1 - 5$, similar to the observed MJO. However, the prescribed single 40-day period is clearly unrealistic. We therefore perform additional sensitivity tests by allowing the speed of the $k = 1$ pattern, c_p, to fluctuate by $\pm$15% around a mean value of 11.6 m/s, as a red-noise process with a 10-day memory (details in the supporting information). As a result, the wavenumber and frequency spectra look more realistic for these sensitivity runs (Figure S1).

Diagnostics. We use two complementary definitions of SSW events, based on reversals and deceleration rates of the polar night jet (PNJ), respectively, following Kim et al. (2017), with details provided in supporting information Text S3. To investigate how the total upward EP flux is affected by the MJO forcing, we decompose the total EP flux into three components: 40-day period waves, stationary waves, and transient waves at frequencies other than 40 days. While 40-day period waves exist in the model also without the 40-day MJO forcing, we assume that the majority of the signal at this frequency is due to this forcing so that this frequency mostly represents the *direct* effect of the forcing. In addition, the forcing changes wave motions at other frequencies, including both stationary waves and transient waves at frequencies other than 40 days, via nonlinear interactions. For details, please refer to supporting information Text S2. While the structure of the simulated unforced SSW events seems fairly realistic in our model, their frequency is two to three events per decade (of perpetual January run) using the reversal criterion and about six per decade using the deceleration criterion. The model thus produces too few events, likely due to the many missing factors in our idealized configuration.

3. Results

Our main objective is to study the interaction between the MJO-forced waves and the midlatitude tropospheric jet and its role in the MJO-SSW teleconnection. We find that window B forcing (corresponding to the location of the observed present-day MJO) leads to absorption of the MJO-forced waves by the midlatitude jet, therefore amplifying the zonal asymmetry of the jet and increasing the upward stationary waves emitted from the midlatitudes. This, in turn, is the dominant mechanism by which the frequency of SSW events is affected. The following subsections explore the different elements of this teleconnection mechanism in detail.

3.1. The Correlation of SSW Frequency With Upward EP Flux

Figures 1c and 1d present the zonal mean climatological temperature responses (forced minus unforced) for two strongly forced cases, A10 and B10. In A10, SSW events are suppressed, and the Arctic stratospheric climatology is cooled by over 8 K, while in B10, which leads to more frequent SSW events, the Arctic stratospheric climatology is warmed by over 6 K. These temperature responses are driven by meridional eddy heat transport, $\overline{v'T'}$, according to the temperature budget (Kang & Tziperman, 2017, not shown).

Proceeding to the response of SSW events, supporting information Figure S2a shows that MJO-like forcings applied within different equatorial longitudinal ranges lead to the SSW frequency either being enhanced (windows A, B, and D) or suppressed (window C into which the MJO is projected to expand in a future warmer climate, and window A at strong amplitudes). The significantly different SSW response to MJO forcing in different longitudinal locations is due to the interaction of the MJO-forced waves with the background zonal asymmetry (Kang & Tziperman, 2018). A qualitatively similar SSW response can be found when using the PNJ deceleration criterion (supporting information Figure S2b). This similarity indicates that the change of the SSW frequency is not merely due to the climatological deceleration of the PNJ but due to the dynamical wave forcing resulting directly and indirectly from the MJO forcing.

The important point to note for the purpose of this paper is that the large-scale ($k = 1, 2$) upward EP flux at the high-latitude tropopause correlates well with the SSW frequency (Figures 1a and 1b). The time mean EP_z shows strong correlation with the SSW frequency based on the wind reversal criterion ($r = 0.91$, Figure 1a) and a somewhat weaker yet still significant correlation with the frequency calculated using the deceleration criterion ($r = 0.59$, Figure 1b).

3.2. Understanding the Midlatitude Jet and Stationary Wave Response to MJO Forcing

We show below (section 3.3) that the upward EP flux response at the high-latitude tropopause shown in Figure 1 is dominated by the change in stationary waves generated in the midlatitudes. We now address our main focus here—the mechanism leading to this change in the midlatitude jet and the corresponding stationary wave response due to the MJO forcing. Figures 2a and 2c show the zonal profiles of the jet-center speed (dashed lines) and of the corresponding deviation of this speed from the unforced simulation (solid lines), for the window B experiments (representing the present MJO) and the window C experiments (corresponding to the region into some of which a future MJO may expand to). Colors from cold to warm denote increasing MJO amplitudes.

The window B and window C forcings both accelerate the jet near the forcing's eastern edge (180°E for B and 300°E for C) and decelerate the jet near the forcing's western edge (60°E for B and 180°E for C), although the acceleration in the window C experiments is weaker. Since the forcing longitudinal location relative

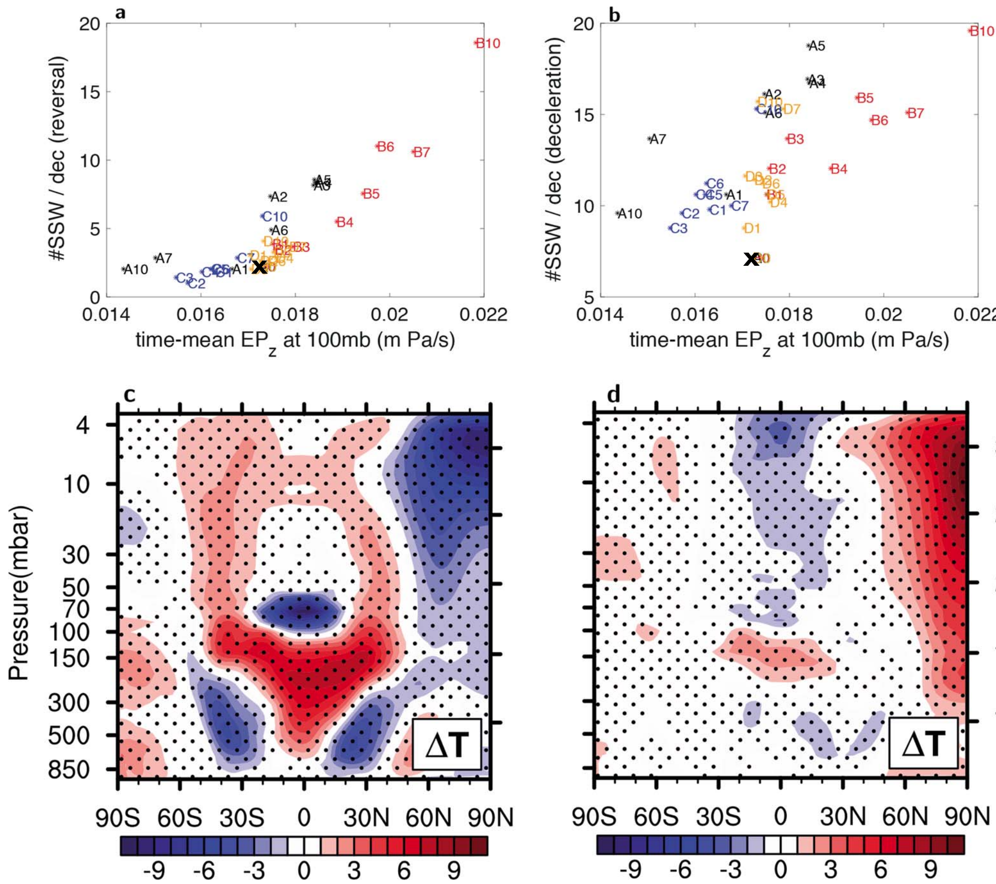

Figure 1. (a) A scatter plot of the number of sudden stratospheric warming (SSW) events per decade as a function of large-scale ($k = 1, 2$) vertical EP flux component, EP_z at the tropopause (100 mb) integrated between 60°N and 90°N. SSWs are identified based on the wind reversal criterion (section 2), and EP_z is time averaged. (b) Similar to (a), except that SSWs are identified based on a polar night jet deceleration criteria (see section 2). Colors indicate the Madden-Julian Oscillation-like forcing window: Black corresponds to window A, red to B, blue to C, and orange to window D. The number following the letter denotes the prescribed maximum forcing heating rate in Kelvin per day. × mark denotes the unforced case. (c, d) Two examples of climatological temperature responses, showing Madden-Julian Oscillation-forced minus Control experiment for A10 (SSWs are suppressed) in (c) and B10 (SSWs are enhanced) in (d).

to the background zonal asymmetry is different in the two windows, window B forcing makes the jet speed more zonally asymmetric, while window C forcing makes it more zonally symmetric, as the MJO amplitude is increased (this is particularly obvious in the strongly forced cases, see Figures 2a and 2c dashed orange line between 0 and 180° E). Supporting information Figure S3 shows that this effect occurs for forcing amplitudes larger than 2–3 K/day.

Figures 2b and 2d show the spatial structure of the forced jet for the strongly forced B10 and C10 experiments. This again shows that forced by strong MJO-like forcing in window B (C), the midlatitude jet becomes more zonally asymmetric (symmetric) and is shifted equatorward (poleward). We note that a more zonally asymmetric jet implies to more stationary waves forced in the jet area, which we find to dominate other wave components and to affect the SSW frequency (next subsection).

To verify that our results are not sensitive to the idealized, single-frequency MJO forcing, we considered the stochastic MJO forcing described in section 2 applied to the B10 and C10 runs and compared to the nonstochastic runs. We find the responses in zonal mean climatology and midlatitude jet to be almost identical (Figure S4). The SSW frequencies in stochastic B10 (C10) are 22 per decade (5.5 per decade), similar to the nonstochastic correspondence, 19 per decade (6 per decade).

The midlatitude jet decelerates everywhere in response to the window D and window A forcings regardless of the forcing amplitude, and when forced by strong (>7 K/day) MJO forcing in window A, the midlatitude

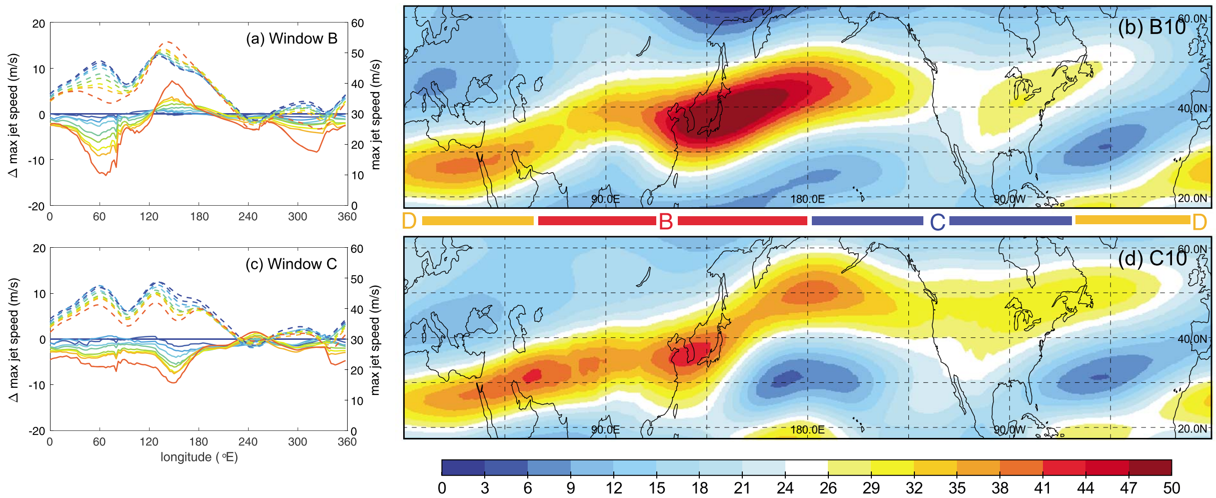

Figure 2. The response of the midlatitude jet to Madden-Julian Oscillation (MJO)-like forcing in window B (a and b) and in window C (c and d). (a and c) Profiles of the maximum jet speed averaged between 20°N and 60°N, at 250 mb, as function of longitude, showing the MJO-forced jet by the dashed lines (right *y* axis), and the forced minus unforced jet response by the solid lines (left *y* axis). The lines varying from cold colors (blue) to warm colors (red) correspond to simulations using weak to strong MJO forcing, at amplitudes of 0, 1, 2, 3, 4, 5, 6, 7, and 10 K/day. (b and d) The U wind field at 250 mb, averaged between 20°N and 60°N, for B window 10-K/day forcing at the top and for C window 10-K/day forcing at the bottom. The forcing ranges of the three longitudinal windows B, C, and D are shown by colored bars between the two panels on the right.

(30°N–60°N) jet decelerates dramatically, forming one jet over the equator (Figure S5). A similar sensitivity of the extratropical response to the location of the stationary tropical forcing was also noticed by Simmons et al. (1983) and Ting and Sardeshmukh (1993).

To understand the different jet responses in the window B and window C experiments, we cannot use the momentum balance of the equilibrated forced runs, as these would simply show a dominantly geostrophic balance, not explaining how the wave forcing modifies the jet structure. An analysis of the PV budget turned out to be noisy and therefore also insufficient for providing insight about the mechanism of the response. We therefore choose to examine the initial response of the jet to the turning on of the forcing. We draw 800 different initial conditions (ICs) from an unforced simulation, at 20-day intervals; then for each IC, we run a 20-day simulation with the strong window B forcing case and a 40-day simulation with the strong window C forcing and take an ensemble average of the responses. The integration lengths are chosen for the two different windows such that a significant part of the equilibrium jet response features is reproduced by the end of the short simulation. The MJO phase at the beginning of each ensemble member is randomly picked, so that the signal associated with any particular MJO phase will be averaged over, and the ensemble average should therefore represent the climatological response of the jet to the MJO forcing.

To diagnose the mechanism of the jet response, we first take the ensemble average (denoted $\langle\cdot\rangle$) and the time average (denoted $\overline{(\cdot)}$) of the zonal momentum equation; we then decompose u and v into the reference state (defined to be the ensemble-mean, time-mean state in the short forced simulations), $\langle\bar{u}\rangle$ and $\langle\bar{v}\rangle$, and the deviation from this reference, u' and v' ($\overline{u'} = \overline{v'} = 0$); finally, we take a mass-weighted vertical average (denoted $[\cdot]$) over the troposphere (100–1,000 mb). The zonal momentum equation becomes

$$\overline{\frac{\partial}{\partial t}\left[\langle u\rangle\right]} + \left[\langle\bar{u}\rangle\frac{\partial\langle\bar{u}\rangle}{\partial x}\right] + \left[\langle\bar{v}\rangle\frac{\partial\langle\bar{u}\rangle}{\partial y}\right] - f\left[\langle\bar{v}_a\rangle\right] = -\frac{\partial}{\partial x}\left[\langle\overline{u'u'}\rangle\right] - \frac{\partial}{\partial y}\left[\langle\overline{u'v'}\rangle\right] + \left[F_0\right], \tag{1}$$

where v_a is the ageostrophic component of the v wind and F_0 is the constant forcing term used to set the background state (see section 2). The time derivative term represents the climatology drift through the 20/40-day integration, which we are trying to explain; that is, $\overline{\partial/\partial t\left[\langle u\rangle\right]} = ([\langle u(T)\rangle] - [\langle u(0)\rangle])/T$, where T is the length of the integration.

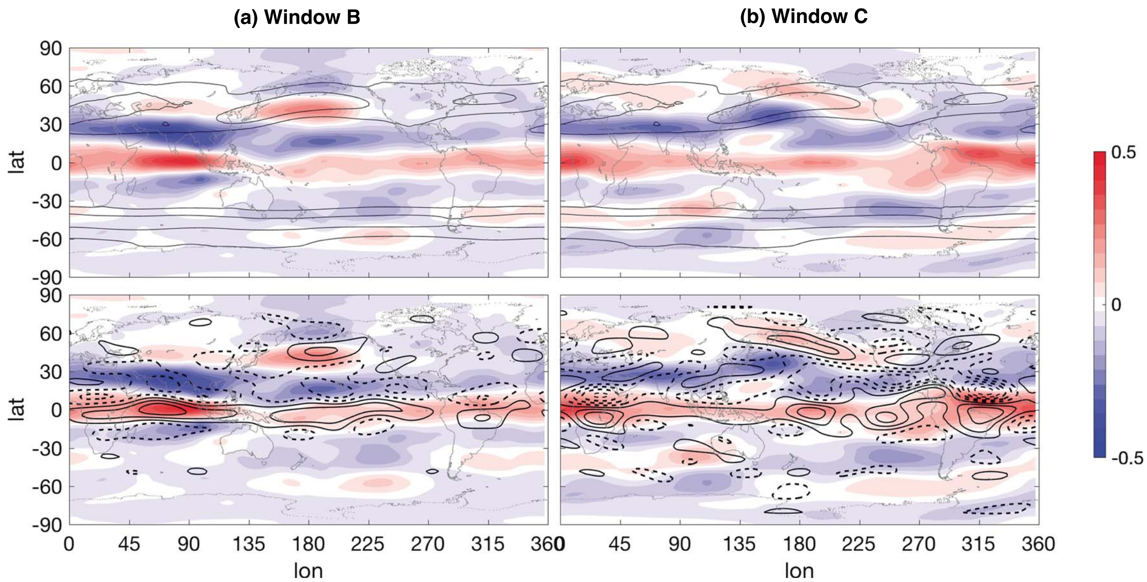

Figure 3. The mechanism of the midlatitude jet response to Madden-Julian Oscillation forcing in different windows. Shown in shadings are the ensemble-averaged forced minus unforced zonal wind field in response to a 10-K/day Madden-Julian Oscillation-like forcing, as shown by the left-hand side of equation (2), for (left) window B after 20 days, and (right) window C after 40 days. The units are m/s/day. The 10- and 20-m/s contours of the unforced zonal wind field are superimposed in the top panels for reference. The meridional eddy flux of zonal momentum, Term 4 in equation (2), is shown by the contours in the bottom panels, showing a good match with the jet response (shading). The contour interval is 0.25 m/s/day, with positive contour values shown by solid lines and negative by dashed lines.

We write the above equation for both the MJO-forced experiment and the unforced experiment and take the difference, denoting forced minus unforced variables by $\hat{(\cdot)}$, and variables from the unforced experiment by a subscript 0,

$$\overbrace{\left[\frac{\langle u(T)\rangle - \langle u(0)\rangle}{T}\right]}^{\text{Term 1}} = \overbrace{\left[-\frac{\partial}{\partial x}\langle\widehat{\overline{u'u'}}\rangle\right]}^{\text{Term 3}} + \overbrace{\left[-\frac{\partial}{\partial y}\langle\widehat{\overline{u'v'}}\rangle\right]}^{\text{Term 4}}$$
$$\underbrace{-\left[\langle\bar{u}_0\rangle\frac{\partial\langle\hat{\bar{u}}\rangle}{\partial x} + \langle\hat{\bar{u}}\rangle\frac{\partial\langle\bar{u}_0\rangle}{\partial x} + \langle\hat{\bar{u}}\rangle\frac{\partial\langle\hat{\bar{u}}\rangle}{\partial x} + \langle\bar{v}_0\rangle\frac{\partial\langle\hat{\bar{u}}\rangle}{\partial y} + \langle\hat{\bar{v}}\rangle\frac{\partial\langle\bar{u}_0\rangle}{\partial y} + \langle\hat{\bar{v}}\rangle\frac{\partial\langle\hat{\bar{u}}\rangle}{\partial y} - f\langle\hat{\bar{v}}_a\rangle\right]}_{\text{Term 2}}. \tag{2}$$

The left-hand side and right-hand side of equation (2) are shown in the top panels of supporting information Figure S6 by shading and contours, respectively, and the close match between the two indicates a closed momentum budget.

The term representing the response of the zonal wind (Term 1, equation (2) is shown by the shading in the top panels of Figure 3, overlaid with contours of the midlatitude jet zonal velocity in the unforced run. By the end of the short simulations, the averages of both short-term experiments reproduce most of the long-term acceleration in the deep tropics, and the deceleration in subtropics, seen in the long-term climatological responses to the B10 and C10 forcing. In the midlatitude, the ensemble experiment for window B (C) reproduces the acceleration (deceleration) around 150°E, the location of the strongest jet, and the equatorward (poleward) shift of midlatitude jet, as observed in the long-term responses.

The meridional eddy momentum transport (Term 4) is shown as contours in the bottom panels of Figure 3, together with the response of the zonal wind (Term 1) shown again by the shading. There is clearly a close correspondence between the two, indicating that the eddy momentum term explains much of the observed jet response. Term 4 accelerates the vicinity of the forced region in the deep tropics and decelerates the zonal wind on both sides of the equator, especially in the north, indicating wave generation near the equator and wave absorption in the subtropics. In the midlatitudes, this term accelerates the jet maximum region in window B, and it decelerates the left wing of the jet maximum and shifts the jet poleward in window C, consistent with the jet response. Therefore, again, it seems that a considerable part of the jet response may be attributed to Term 4, the meridional eddy momentum transport. These transient eddies were also shown to play a dominant role in the extratropical response to stationary tropical forcing (such as due to El Niño, Held et al., 1989) and to affect the Arctic surface temperature by driving a meridional circulation (Yoo et al., 2012).

All terms on the right-hand side of equation (2) are shown in supporting information Figure S6 to be large compared with the left-hand side term showing the response of the jet, and there are significant cancelations between them, highlighting the complexity of the jet response. While the meridional eddy momentum flux does seem the strongest candidate for explaining the jet response based on its spatial structure, the results are still noisy, and a more complete understanding of this response may require using a yet simpler model, perhaps along the lines of the shallow water model study of Bao and Hartmann (2014).

Ensemble members are quite different, because each member starts from a different initial condition and is forced by a different MJO initial phase. However, the ensemble mean, which is the important quantity as far as the long-term interaction of the jet and the MJO is concerned, is very robust: recalculating the ensemble average using 320 additional initial conditions for window B, taken from an extension of the control run, leads to nearly identical results (Figure S7).

To summarize, the MJO forcing leads to eddy momentum fluxes that change the jet structure, making it more asymmetric for window B and less asymmetric for window C. This leads to more stationary waves emitted from the jet region in window B and less in C, which then explains the larger increase in the SSW frequency in the window B experiments.

3.3. The Dominance of Stationary Wave Response and Partial Cancelation Due To Transient Wave Response

We now show that the response to MJO forcing of the total large-scale EP_z at the Arctic tropopause, which we showed to be correlated with the SSW frequency response (Figure 1a), is dominated by the response of stationary waves produced in the midlatitude jet region. This is explained by the changes to the zonal asymmetry of the midlatitude jet discussed in the previous subsection. First, Figures 4a and 4b (complemented by supporting information Figure S8) show that although the SSW frequency is most enhanced in B window experiments, the EP flux at the Arctic tropopause contributed by directly MJO-forced 40-day period waves is quite low compared to that forced by other windows. (Compare red dashed lines in Figures 4a and 4b). At the same time, the stationary waves emitted from midlatitudes in experiment B are significantly strengthened (orange dashed lines), leading to a total increase in the upward EP flux seen by the stratosphere and therefore to the enhanced SSW frequency.

The generation and initial propagation of the directly MJO-forced 40-day period waves is insensitive to the MJO window location: the relative difference of the 100- to 800-mb integrated EP_y at 25°N is at most 30% among the B, C, and D window experiments (not shown). Therefore, the difference in the transmission rate between different windows is due to two factors. First, different longitudinal windows of the wave source would lead to an interaction with the jet at different longitudes and therefore to different transmission rates. Second, the transmission is also affected by the nonlinear interaction between these waves and the background zonal asymmetry (e.g., the jet exit). Bao and Hartmann (2014) analyzed a shallow water model and noticed a quasi-stationary response to an idealized MJO forcing, corresponding to the change to the jet observed in our window B experiments.

Finally, consider the wave components responsible for the forced changes to the EP flux at the tropopause, which causes the SSW frequency changes analyzed above. Figure 4c shows that the EP_z due to transient waves that were not directly forced by the MJO (section 2) is negatively correlated with the stationary EP_z at the Arctic tropopause (60°–90°N, 100 mb). Figure 4d shows it to be positively correlated with the upper tropospheric (300 mb) zonal wind speed at similar latitudes, which is proportional to the meridional temperature gradient, that is, the baroclinicity. Both correlation coefficients are greater than 0.90 and insensitive to the choice of latitude bands used for the averaging. This suggests that the stationary waves affect the midlatitude jet and baroclinicity (previous subsection), and this, in turn, reduces the production of transient waves at midlatitudes. This cancelation of transient versus stationary waves causes the total EP_z at the Arctic tropopause to changes by only 34% of the change in stationary EP_z there. While the change in baroclinicity is consistent with the effect on the non-MJO-related transient waves, we did not rule out the possibility that these transient waves react somehow directly to the MJO forcing, rather than being reduced indirectly via the change to the baroclinicity.

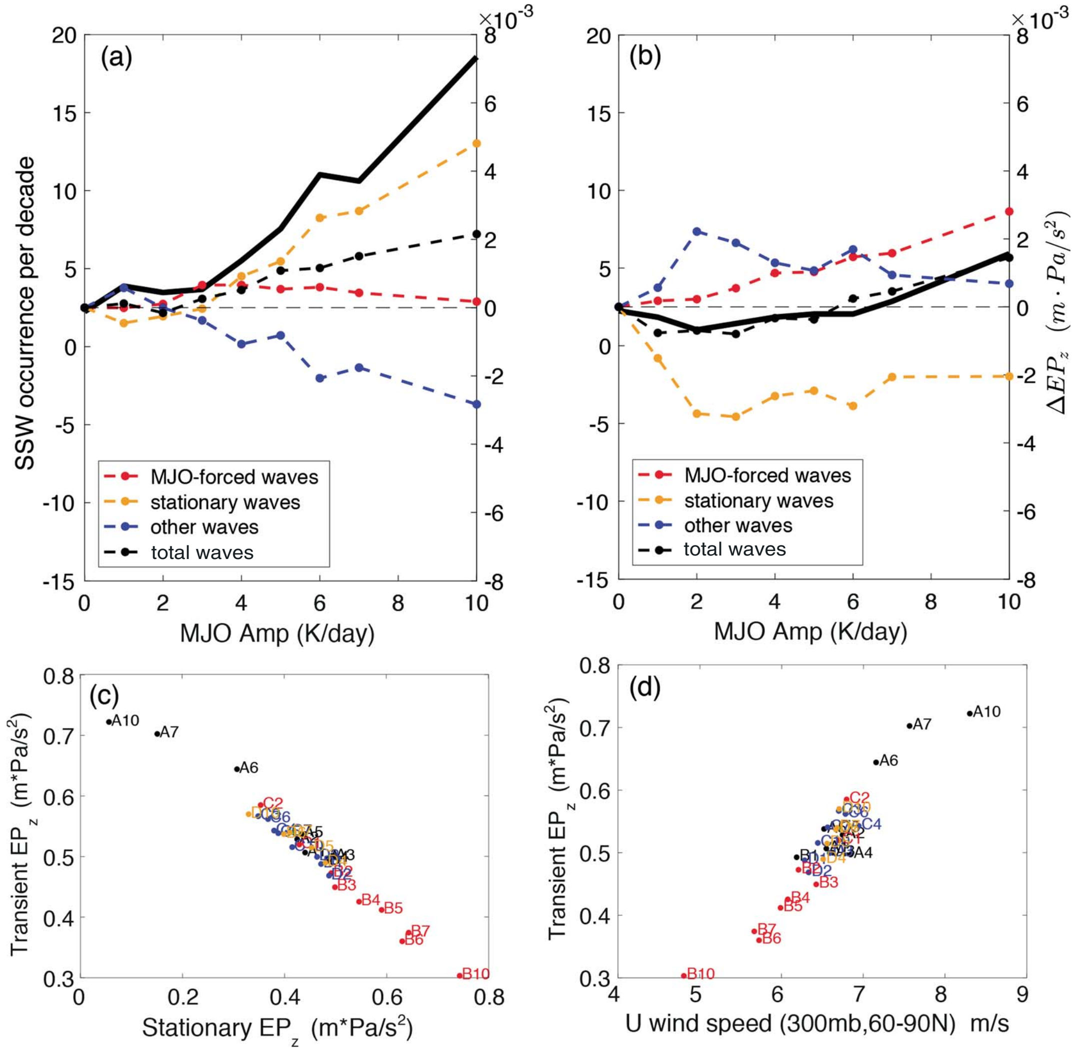

Figure 4. The response of stationary versus transient waves to Madden-Julian Oscillation (MJO)-like forcing. (a) Response to B window forcing: Number of SSW events per decade (thick solid black line, left axis) and the vertical component of the large-scale EP flux at the tropopause, integrated over 60°N–90°N, for forced minus unforced experiments (dashed lines, right axis): (red) EP flux associated with directly MJO-forced 40-day period waves; (orange) EP flux associated with large-scale stationary wave; (black) total large-scale EP flux, where anomalies are filtered by wavenumbers 1 and 2; (blue) EP flux due to "other waves," calculated by subtracting the directly MJO-forced 40-day period waves (red) and the stationary waves (orange) from the total (black) EP flux. See section 2 for details. (b) Same as (a), for window C. (c) A scatter plot of the contribution of transient waves to the Arctic tropopause EP_z flux (m/Pa s), against the contribution of large-scale stationary wave to the Arctic tropopause EP_z. (d) A scatter plot of the contribution of transient waves to the Arctic tropopause EP_z flux (m/Pa s) against the zonal mean zonal wind at 300 mb. Both EP_z and the zonal mean zonal wind are averaged over 60°–90°N. Each dot represents one experiment, with the experiment name labeled. Different colors are used to distinguish the experiments with different MJO windows (black: window A, red: window B, blue: window C, and orange: window D).

4. Conclusions

The MJO is projected to be stronger and expand to a larger longitudinal range in a warmer climate (Arnold et al., 2013, 2014; Chang et al., 2015; Jones & Carvalho, 2006; Lee, 1999; Slingo et al., 1999). We used a dry dynamical core model to investigate how MJO-like forcing, with different longitudinal ranges and amplitudes, affects the frequency of SSW, especially focusing on the interaction between the midlatitude jet and the MJO-like forcing.

We first showed a strong correlation between the SSW frequency and the large-scale EP_z at the Arctic tropopause, in response to MJO forcing with varying amplitudes and longitudinal ranges. Thus, in order to explain the SSW response, we need to explain the changes to this high-latitude vertical EP flux. It is known that the midlatitude tropospheric jet structure can control both the propagation of equatorially forced waves (e.g., Kang & Tziperman, 2018) and the generation of stationary waves there, and we therefore focused here on the analysis of the mechanism of this midlatitude jet response. We showed that MJO-forced eddy meridional flux of zonal momentum ($\overline{u'v'}$) is the dominant forcing causing the jet response. Specifically, MJO forcing at the longitudinal range corresponding to present-day forcing causes an increase to the zonal asymmetry of the jet, therefore strengthening the stationary waves generated in the jet region and increasing the SSW frequency. We also showed that MJO-like forcing applied at other longitudes can have an opposite effect, highlighting the importance of future changes in not only the MJO amplitude but also its longitudinal range. We then decomposed the total large-scale EP_z flux in the Arctic tropopause into contributions due to the directly MJO-forced 40-day period waves, transient waves at other frequencies that are forced nonlinearly by the MJO, and stationary waves generated in the midlatitudes. The increase in stationary waves was found to dominate the effect on SSW events yet to be partially canceled by a decrease in transient waves not directly forced by the MJO. We show indications that these transient waves are weakened due to a reduction of the midlatitude meridional temperature gradient (baroclinicity) by the MJO forcing.

This work demonstrated the complex interplay between MJO forcing, the midlatitude jet, midlatitude-generated stationary and transient eddies, and the SSW frequency and explored the relevant physical mechanisms. We noted that the mechanism of the jet response is complex and that further studies, perhaps using even more idealized models, are needed to deepen our understanding of this problem. This work focused on the anticipated strengthening of the MJO in a warmer climate but did not take the expected change of the static stability, storm track, and other general circulation features into account. Such changes may affect the Arctic stratosphere directly and may also change the way the MJO impacts SSWs. Future work will need to consider not only changes to the MJO but also many other intervening factors that may change in response to a global warming (e.g., blocking events, stationary wave patterns, storm track structure, El Niño–Southern Oscillation, and Quasi-Biennial-Oscillation; Cohen & Jones, 2011; Garfinkel et al., 2010; Kretschmer et al., 2017; Martius et al., 2009; Polvani & Waugh, 2004).

Acknowledgments
This work was supported by the NSF P2C2 program, grant OCE-1602864 and by the Harvard Global Institute and Harvard Climate Solutions funds. E. T. thanks the Weizmann Institute for its hospitality during parts of this work. We would like to acknowledge high-performance computing support from Yellowstone provided by NCAR's Computational and Information Systems Laboratory, sponsored by the National Science Foundation. Model parameter files and analysis scripts used to generate model output and analyze it are available on the authors' web page, under http://www.seas.harvard.edu/climate/eli/Downloads/MJO-SSW/.

References

Adames, Á. F., Kim, D., Sobel, A. H., Del Genio, A., & Wu, J. (2017). Changes in the structure and propagation of the MJO with increasing CO_2. *Journal of Advances in Modeling Earth Systems*, *9*(2), 1251–1268. https://doi.org/10.1002/2017MS000913

Arnold, N., Branson, M., Burt, M. A., Abbot, D. S., Kuang, Z., Randall, D. A., & Tziperman, E. (2014). Effects of explicit atmospheric convection at high CO_2. *Proceedings of the National Academy of Sciences of the United States of America*, *111*(30), 10,943–10,948. https://doi.org/10.1073/pnas.1407175111

Arnold, N., Kuang, Z., & Tziperman, E. (2013). Enhanced MJO-like variability at high SST. *Journal of Climate*, *26*, 988–1001. https://doi.org/10.1175/JCLI-D-12-00272.1

Bao, M., & Hartmann, D. L. (2014). The response to MJO-like forcing in a nonlinear shallow-water model. *Geophysical Research Letters*, *41*, 1322–1328. https://doi.org/10.1002/2013GL057683

Brayshaw, D. J., Hoskins, B., & Blackburn, M. (2009). The basic ingredients of the North Atlantic storm track. Part I: Land–sea contrast and orography. *Journal of the Atmospheric Sciences*, *66*(9), 2539–2558. https://doi.org/10.1175/2009jas3078.1

Brayshaw, D. J., Hoskins, B., & Blackburn, M. (2011). The basic ingredients of the North Atlantic storm track. Part II: Sea surface temperatures. *Journal of the Atmospheric Sciences*, *68*(8), 1784–1805. https://doi.org/10.1175/2011jas3674.1

Chang, C. W. J., Tseng, W. L., Hsu, H. H., Keenlyside, N., & Tsuang, B. J. (2015). The Madden-Julian Oscillation in a warmer world. *Geophysical Research Letters*, *42*, 6034–6042. https://doi.org/10.1002/2015GL065095

Cohen, J., & Jones, J. (2011). Tropospheric precursors and stratospheric warmings. *Journal of Climate*, *24*(24), 6562–6572. https://doi.org/10.1175/2011JCLI4160.1

Craig, R. A., Hering, W. S., Craig, R. A., & Hering, W. S. (1959). The stratospheric warming of January–February 1957. *Journal of the Meteorology*, *16*(2), 91–107. https://doi.org/10.1175/1520-0469(1959)016<0091:TSWOJF>2.0.CO;2

Garfinkel, C. I., Feldstein, S. B., Waugh, D. W., Yoo, C., & Lee, S. (2012). Observed connection between stratospheric sudden warmings and the Madden-Julian Oscillation. *Geophysical Research Letters*, *39*, L18807. https://doi.org/10.1029/2012GL053144

Garfinkel, C. I., Hartmann, D. L., & Sassi, F. (2010). Tropospheric precursors of anomalous Northern Hemisphere stratospheric polar vortices. *Journal of Climate*, *23*(12), 3282–3299.

Hall, N. (2000). A simple GCM based on dry dynamics and constant forcing. *Journal of the Atmospheric Sciences*, *57*(10), 1557–1572. https://doi.org/10.1175/1520-0469(2000)057<1557:ASGBOD>2.0.CO;2

Held, I. M., Lyons, S. W., & Nigam, S. (1989). Transients and the extratropical response to El Niño. *Journal of the Atmospheric Sciences*, *46*, 163–174.

Jones, C., & Carvalho, L. M. V. (2006). Changes in the activity of the Madden-Julian Oscillation during 1958–2004. *Journal of Climate*, *19*, 6353–6370.

Kang, W., & Tziperman, E. (2017). More frequent sudden stratospheric warming events due to enhanced MJO forcing expected in a warmer climate. *Journal of Climate*, *30*(21), 8727–8743. https://doi.org/10.1175/JCLI-D-17-0044.1

Kang, W., & Tziperman, E. (2018). The role of zonal asymmetry in the enhancement and suppression of sudden stratospheric warming variability by the Madden-Julian Oscillation. *Journal of Climate*, *31*(6), 2399–2415. https://doi.org/10.1175/JCLI-D-17-0489.1

Kim, J., Son, S.-W., Gerber, E. P., & Park, H.-S. (2017). Defining sudden stratospheric warming in climate models: Accounting for biases in model climatologies. *Journal of Climate*, *30*(14), 5529–5546. https://doi.org/10.1175/JCLI-D-16-0465.1

Kolstad, E. W., Breiteig, T., & Scaife, A. A. (2010). The association between stratospheric weak polar vortex events and cold air outbreaks in the Northern Hemisphere. *Quarterly Journal of the Royal Meteorological Society*, *136*(649), 886–893. https://doi.org/10.1002/qj.620

Kretschmer, M., Runge, J., & Coumou, D. (2017). Early prediction of extreme stratospheric polar vortex states based on causal precursors. *Geophysical Research Letters*, *44*, 8592–8600. https://doi.org/10.1002/2017GL074696

Lee, S. (1999). Why are the climatological zonal winds easterly in the equatorial upper troposphere? *Journal of the Atmospheric Sciences*, *56*(10), 1353–1363.

Limpasuvan, V., Thompson, D., & Hartmann, D. (2004). The life cycle of the Northern Hemisphere sudden stratospheric warmings. *Journal of Climate*, *17*(13), 2584–2596.

Liu, C., Tian, B., Li, K.-F., Manney, G. L., Livesey, N. J., Yung, Y. L., & Waliser, D. E. (2014). Northern Hemisphere mid-winter vortex-displacement and vortex-split stratospheric sudden warmings: Influence of the Madden-Julian Oscillation and Quasi-Biennial Oscillation. *Journal of Geophysical Research: Atmospheres*, *119*, 12,599–12,620. https://doi.org/10.1002/2014JD021876

Marsh, D. R., Mills, M. J., Kinnison, D. E., Lamarque, J.-F., Calvo, N., & Polvani, L. M. (2013). Climate change from 1850 to 2005 simulated in CESM1 (WACCM). *Journal of Climate*, *26*(19), 7372–7391. https://doi.org/10.1175/JCLI-D-12-00558.1

Martius, O., Polvani, L. M., & Davies, H. C. (2009). Blocking precursors to stratospheric sudden warming events. *Geophysical Research Letters*, *36*, L14806. https://doi.org/10.1029/2009GL038776

Mitchell, D. M., Gray, L. J., Anstey, J., Baldwin, M. P., & Charlton-Perez, A. J. (2013). The influence of stratospheric vortex displacements and splits on surface climate. *Journal of Climate*, *26*(8), 2668–2682. https://doi.org/10.1175/JCLI-D-12-00030.1

Naoe, H., Matsuda, Y., & Nakamura, H. (1997). Rossby wave propagation in idealized and realistic zonally varying flows. *Journal of the Meteorological Society of Japan*, *75*(3), 687–700.

Obrien, E., Stewart, D. A., & Branscome, L. E. (1994). Tropical extratropical interactions on intraseasonal time scales in a global spectral model. *Journal of the Atmospheric Sciences*, *51*(10), 1244–1260. https://doi.org/10.1175/1520-0469(1994)051<1244:TIOITS>2.0.CO;2

Polvani, L. M., & Waugh, D. W. (2004). Upward wave activity flux as a precursor to extreme stratospheric events and subsequent anomalous surface weather regimes. *Journal of Climate*, *17*(18), 3548–3554. https://doi.org/10.1175/1520-0442(2004)017<3548:UWAFAA>2.0.CO;2

Simmons, A. J., Wallace, J. M., & Branstator, G. W. (1983). Barotropic wave propagation and instability, and atmospheric teleconnection patterns. *Journal of the Atmospheric Sciences*, *40*(6), 1363–1392. https://doi.org/10.1175/1520-0469(1983)040<1363:bwpaia>2.0.co;2

Slingo, J., Rowell, D., Sperber, K., & Nortley, E. (1999). On the predictability of the interannual behaviour of the Madden-Julian Oscillation and its relationship with El Niño. *Quarterly Journal of the Royal Meteorological Society*, *125*(554, Part B), 583–609. https://doi.org/10.1002/qj.49712555411

Tamarin, T., & Kaspi, Y. (2017). Mechanisms controlling the downstream poleward deflection of midlatitude storm tracks. *Journal of the Atmospheric Sciences*, *74*(2), 553–572.

Thompson, D. W. J., Baldwin, M. P., & Wallace, J. M. (2002). Stratospheric connection to Northern Hemisphere wintertime weather: Implications for prediction. *Journal of Climate*, *15*(12), 1421–1428. https://doi.org/10.1175/1520-0442(2002)015<1421:SCTNHW>2.0.CO;2

Ting, M. F., & Sardeshmukh, P. D. (1993). Factors determining the extratropical response to equatorial diabatic heating anomalies. *Journal of the Atmospheric Sciences*, *50*(6), 907–918. https://doi.org/10.1175/1520-0469(1993)050<0907:FDTERT>2.0.CO;2

Webster, P. J., & Chang, H.-R. (1988). Equatorial energy accumulation and emanation regions: Impacts of a zonally varying basic state. *Journal of the Atmospheric Sciences*, *45*(5), 803–829. https://doi.org/10.1175/1520-0469(1988)045<0803:EEAAER>2.0.CO;2

Yoo, C., Lee, S., & Feldstein, S. B. (2012). Arctic response to an MJO-like tropical heating in an idealized GCM. *Journal of the Atmospheric Sciences*, *69*(8), 2379–2393. https://doi.org/10.1175/JAS-D-11-0261.1